ELSEVIER

Journal of Molecular Catalysis A: Chemical 119 (1997) 77–85

JOURNAL OF MOLECULAR CATALYSIS A: CHEMICAL

Structural characterization of NiO doped with several caesium loadings

Rosa Fernández [a], Joaquim Estelle [a], Yolanda Cesteros [a], Pilar Salagre [a], Francisco Medina [b], Jesús-Eduardo Sueiras [b,*], Jose-Luis Garcia Fierro [c]

[a] *Facultat de Química, Universitat Rovira i Virgili, Pl. Imperial Tarraco 1, 43005 Tarragona, Spain*
[b] *Escola Tècnica Superior d'Enginyeria, Universitat Rovira i Virgili, Pl. Imperial Tarraco 1, 43005 Tarragona, Spain*
[c] *Instituto de catálisis y Petroleoquímica, CSIC, Campues UAM Cantoblanco, 28049 Madrid, Spain*

Received 4 June 1996; accepted 24 July 1996

Abstract

Several samples obtained from doping NiO with different loading amounts of caesium oxide were structurally characterized using BET, TPR, XRD, XPS and SEM techniques. From BET results, increasing caesium contents decrease surface areas except at temperatures with partial reduction. TPR shows that high caesium loadings can promote NiO reduction at the beginning of its reduction contrarily to previously reported potassium behaviors, and also a reduction inhibiting counter-effect at the end of the reduction curves with the same increasing caesium loadings. XRD and SEM clearly show differentiated crystalline morphologies on the oxidized and reduced caesium-doped nickel phases obtained from the solids studied. XPS results show the reducibility behaviour of the solid surfaces confirming the NiO reduction promoting effect with increasing caesium loadings and also a dramatic caesium migration towards the surface of the solids mainly at initial reduction temperatures. That abundant surface caesium content delays the complete reduction of the solids.

Keywords: Caesium; Nickel catalysts; Characterization

1. Introduction

The addition of small amounts of alkali has long been known to modify the activity and the selectivity of heterogeneous catalysts [1,2]. One of the interpretations of alkali doping is usually thought in terms of electronic effects. The additive is considered as a base, transferring electrons to the metallic phase, thus increasing the bond strength of electron-acceptor molecules such as CO, N_2 and decreasing that of electron-donor molecules such as hydrogen [3,4].

Potassium addition to Ni/SiO_2 is claimed to block a certain number of Ni atoms, to act as an electronic modifier of the remaining free Ni atoms, and to strength bonds with electronegative molecules and ethylenics [5].

Doping potassium, onto Ni/SiO_2, from their calcined and reduced salts is described as mainly present in a K–O–Ni surface complex concentrated on the nickel surface into patches or islands leaving another part of the potassium (also in an oxidized form) fixed onto the silica support [6].

* Corresponding author.

PII S1381-1169(96)00471-2

Partial decoration of the Pd surface by the ionic alkali compound in Pd/SiO_2 solids was also reported [7]. Large decreases of CO stretching frequencies and modifications of catalytic properties in alkali doped Pd/SiO_2 were claimed [8]. The effect of alkali promoters on the increase of activity and selectivity of Pd/Al_2O_3 catalysts was reported for the hydrogenation of phenol [9].

Potassium addition is known to enhance the selectivity of nickel catalysts towards primary amines obtained from adiponitrile hydrogenations [10–13], to increase selectivities toward heavy hydrocarbons and olefinic compounds in the $CO + H_2$ reaction [1,3,14–16], to inhibit hydrogenolysis over Ni and Fe [17], to improve the performance of Fe or Ru-based catalysts for ammonia synthesis [18,19]. Nickel–potassium catalysts are also used for steam-reforming of methane or naphtha [20], and for coal gasification [21].

Alkali additives may also act as structural promoters, preventing sintering of the metallic phase. Stabilities varying according to the sequence $K > Na > Li >$ unpromoted Ni/SiO_2 were reported [22]. Doping was found to strongly influence the kinetics of thermal decomposition of nickel carbonates [23]. Stabilization effects of potassium on Pd/SiO_2 catalysts were also reported [24].

As far as unsupported metals are concerned potassium turns out to be again the most studied alkali additive, as in the effect on the reducibility of metal oxides [25,26], in theoretical studies about the electronic properties of a nickel (111) surface partially covered by potassium adatoms [27], the effect of potassium/sodium doped Pt(100) single crystals on the activity and selectivity for the 1,3-butadiene hydrogenation [28].

However, even expecting lower doped-metal 'local' work functions with promoters more electropositive than potassium, little has been published concerning the promotion behaviour of caesium [29], specially on catalysts for nitrile hydrogenation, as far as structural, catalytic and mechanistic features are concerned. In this work we study several structural effects of doping nickel with caesium, of potential interest in catalytic hydrogenation reactions.

2. Experimental

2.1. Sample preparation

Non-doped and caesium-doped nickel precursors were prepared by impregnation of the previously calcined nickel nitrate hexahydrate with the relevant doping amounts of caesium nitrate aqueous solutions, as shown in Table 1, and ulterior drying at 393 K for 5 h. All samples were reduced (reactor conditions) with hydrogen/argon for 20 h, with a 1/20 volume ratio, an initial space velocity of 360 h^{-1} (with respect to the active gas), and temperatures shown in Table 1. These preparations will be designated hereafter as samples 1–14, respectively.

All reagents were reagent-grade (from Aldrich Co.), and pure gases were previously dried and deoxygenated.

2.2. Air-free sampling

The samples were always handled under air-free conditions, after the reduction step. The prepared solids were transferred in degassed *iso*-octane and under hydrogen atmosphere at room temperature. The *iso*-octane surface-impregnated samples were further isolated from the air with sticky tape and mounted in a glove box for XRD monitoring. Alternatively, they were vacuum pumped in the pre-evacuation chamber of the photoelectronspectrometer, resulting in neither significant carbon contamination nor air oxidation from this procedure. Gas purges, positive gas pressures and Schlenk techniques were used when necessary.

2.3. BET areas

BET surface areas were calculated from the nitrogen adsorption isotherms at 77 K using a

Table 1
Specific surface area and XRD characterization of the catalysts

Sample [a]	g Cs_2O/g Ni ($\times 10^{-3}$)	Reduction temperature (K)	BET area (m^2/g)	Crystal phases in the reduced sample (XRD)
1	0	–	9.0	NiO
2	0	573	1.2	Ni
3	1	–	6.1	NiO
4	1	473	5.8	NiO, Ni
5	1	523	2.4	Ni
6	1	573	2.1	Ni
7	2	–	5.8	NiO
8	2	473	4.4	NiO, Ni
9	2	523	1.5	Ni
10	2	573	1.5	Ni
11	3	–	5.1	NiO
12	3	473	8.1	NiO, Ni
13	3	523	2.3	Ni
14	3	573	2.0	Ni

[a] Calcined samples 1, 3, 7 and 11 were not subjected to reduction.

Micromeritics ASAP 2000 surface analyzer, and a value of 0.164 nm^2 for the cross section of the nitrogen molecule.

2.4. Temperature programmed reduction (TPR)

Temperature programmed reductions were carried out in a Perkin-Elmer TGA 7 microbalance with an accuracy of 1 mg, equipped with a 273–1273 K programmable temperature furnace. 25 mg samples were first heated at 4 K min^{-1} up to 673 K in a stream of He (80 cm^3 min^{-1}) for moisture release. After cooling to room temperature under helium, they were heated again in a 5% vol H_2/Ar flow (80 cm^3 min^{-1}) up to reduction temperatures, between 443–623 K. The weight change in the samples is a measure of the oxygen released by the solid as water.

2.5. X-ray diffraction (XRD)

Powder X-ray diffraction (XRD) patterns of the catalysts were obtained with a Philips PW 1010 diffractometer using nickel-filtered Cu K_α radiation. Samples were dusted on double-sided sticky tape and mounted on glass microscope slides. The patterns were recorded over a range of 20 angles from 5° to 85° and compared with the X-ray powder files to confirm phase identities. The reduced samples characterized by XRD were obtained under the reactor conditions given in the preparation section.

2.6. Scanning electron microscopy (SEM)

Scanning electron micrographs were obtained in a JEOL JSM-35C microscope operating at acceleration voltages 25 kV, working distances 18–19 mm and magnification values of $\times$25.000–40.000.

2.7. X-ray photoelectron spectroscopy (XPS)

X-ray photoelectron spectra were recorded on a Leybold LHS 10 spectrometer provided with a hemispherical energy analyzer and Mg K_α X-ray radiation source. Powdered samples were pressed into small stainless steel cylinders and mounted on a standard sample probe, placed in a pre-evacuation chamber up to ca. 10^{-5} Torr, before they were moved into the main vacuum chamber. The oxide samples for XPS characterization were subjected to a short reduction treatment (2 h and same conditions given in the preparation section) in order to better detect

property changes. The residual pressure in the turbo-pumped analysis chamber was kept below 7×10^{-9} Torr during data collection. Each spectral region was signal-averaged for a given number of scans to obtain good signal-to-noise ratios. Although surface charging was observed on all the samples, accurate binding energies (BE) were determined by charge referencing with the C1s line at 284.6 eV. Peak areas of Ni(0) and Ni(II) including satellites, were computed by a program which assumed Gaussian-line shapes and flat background subtraction.

3. Results and discussion

3.1. BET areas

Table 1 depicts the BET areas of the undoped and caesium-doped solids obtained. Values between 1.5–9 m^2/g are typical for samples prepared under the conditions mentioned above [12,25,26]. Generally, decreasing areas on increasing the reduction temperatures of the samples are obtained, paralleling the increases of the reduction degrees with temperature, for the sets of samples 1–2, 3–6, 7–10 and 11–14, (except for sample 12 with the higher caesium content and lower reduction temperature, which brings about a low degree of reduction and consequently a higher surface area) since the area of the unreduced non-stoichiometric, black NiO (sample 1) has more than four-fold the area of its reduced Ni form (sample 2) and, to a decreasing extent is also true for every set of the caesium-doped samples. The range of caesium concentrations on the NiO samples tested, always delay or inhibit the complete reduction of NiO, as we will see from the TPR experiments below.

Also, from Table 1, increasing caesium contents cause parallel decreases of the surface areas of the samples, at one particular reduction temperature (except for samples 12–14 because of the reason given before). For equal final reduction degrees, decreasing surface areas are

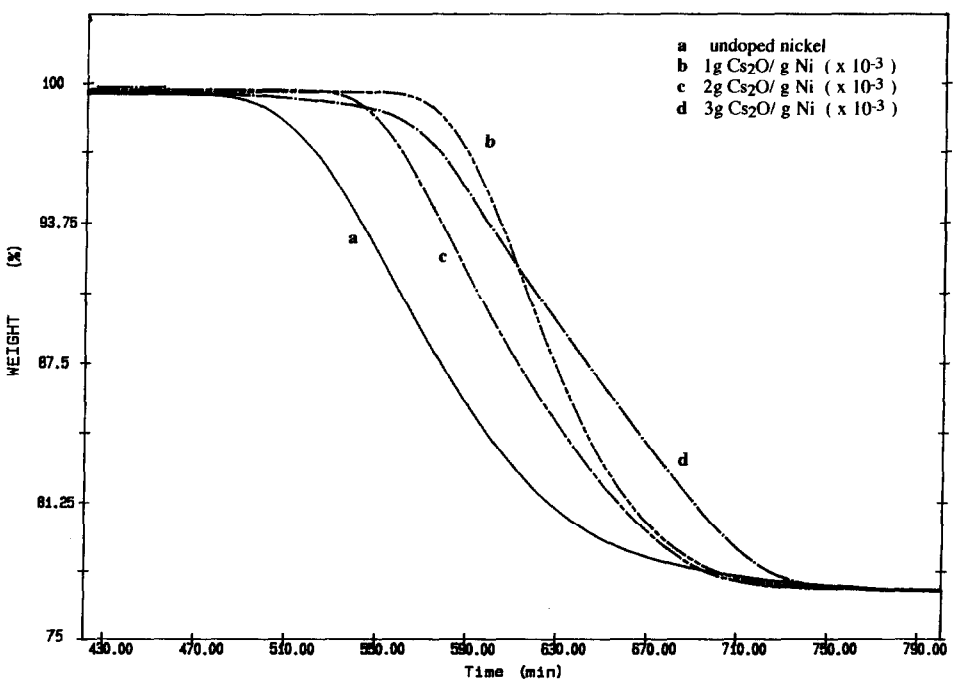

Fig. 1. Plot of weight change (%) versus time for the temperature programmed reduction of undoped NiO and caesium-doped NiO samples. Initial temperature 393 K; rate of heating 0.2 K min^{-1}.

obtained from increasing caesium contents, since caesium, unlike potassium, shows an extremely high hygroscopy and a strong migration behaviour towards the surface of the solid, as it will be shown from the XPS experiments, below.

3.2. Temperature programmed reduction

To perform the study of the caesium role on the reducibility of non-stoichiometric NiO, the corresponding hydrogen-reduction thermograms were obtained. Fig. 1 shows the weight decrease versus time of the caesium-doped NiO samples compared with that of the undoped NiO. We should say that all samples after a long drying procedure did not show the presence of water other than that from the stoichiometric reduction. It can be observed, for the caesium-doped NiO samples, that the initial temperature of reduction decreases in parallel with the increase of the caesium content. As well, the sample which has the highest caesium amount (3×10^{-3} g Cs_2O/g Ni) shows an initial temperature of reduction slightly lower than the undoped NiO as shown in Fig. 2.

On the other hand, the final temperatures of reduction increase with caesium contents, being higher than that of the undoped NiO sample.

The trend obtained from the initial temperatures of reduction may be indicative of an electronic promoting function of caesium that accelerates the NiO reducibility with increasing caesium contents. However, one or more counter-effects derived from the impeded hydrogen and water diffusions, due to the surface bulky and hygroscopic caesium oxide which obstructs and delays the final reduction of the caesium-doped samples, are also present. The latter effect may be responsible for the crossing behavior obtained between the initial and final reduction portions of the TPR curves, and also for the longer time shifts obtained for the caesium-doped samples when compared with that from the undoped NiO sample.

Fig. 3 shows the degree of reduction versus temperature for caesium-doped NiO and undoped NiO samples. The S-shaped reduction

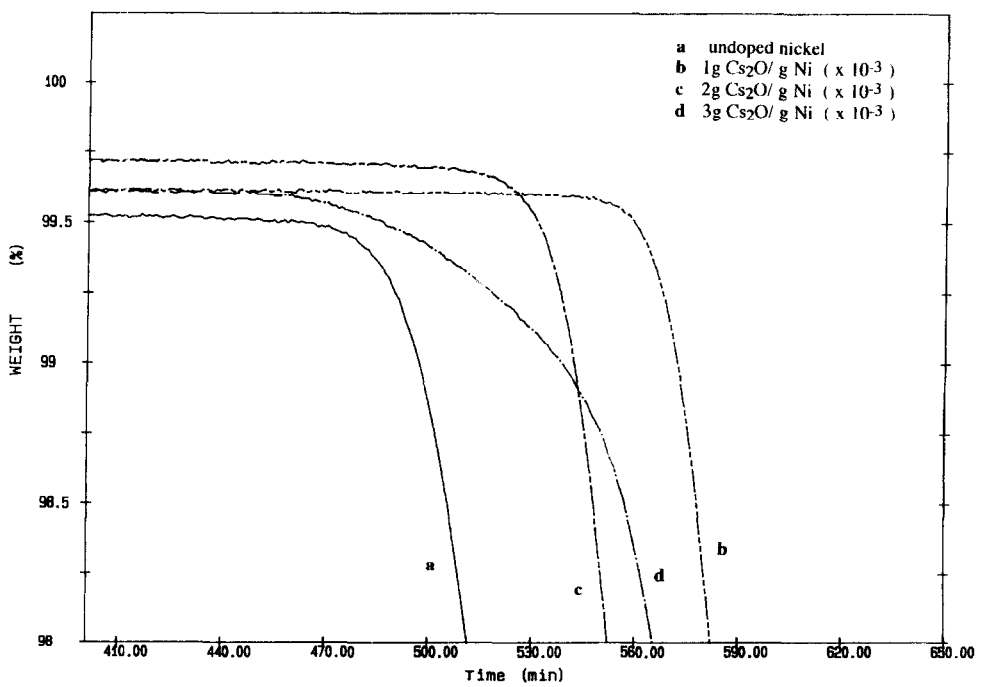

Fig. 2. Fig. 1 magnification plot at lower weight loss.

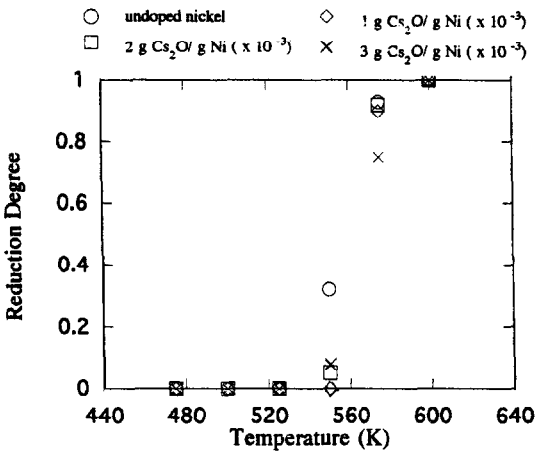

Fig. 3. Plot of reduction degree (α) versus temperature of undoped NiO and caesium-doped NiO samples.

plots are in agreement with the nucleation model of the nickel oxide reduction, where an autocatalytic process of metallic nucleus growth takes place on the surface of nickel oxide with the increase of reduction [21,26]. Thus, the addition of caesium does not modify the mechanism of the oxide reduction, and can also explain the diffusion problems in the nucleation step, and final reduction delay of sample 11.

3.3. X-ray diffraction

Powder diffraction patterns of the reduced samples showed diffraction peaks at 2Θ angles and relative intensities which can be indexed to the Ni and NiO phases. The 2Θ angles and the relative intensities (in parentheses) are summarized as follows: 44.51 (100), 51.85 (42), 76.36 (21), for the Ni phase; 37.29 (91), 43.30 (100), 62.91 (57), 75.43 (16), for the NiO phase. Caesium phases were undetectable owing to their very low concentrations.

The crystalline phases in Table 1 were obtained at different temperatures of reduction of undoped and caesium-doped nonstoichiometric NiO. The reduced Ni phases obtained at 473°C from the mid and lower caesium loadings and the mixture of phases NiO/Ni obtained at the same temperature for the higher caesium loading tested, indicate that reduction temperature of Nio needs rise in the presence of doping caesium contents. The BET areas depicted in Table 1 also confirms this behavior showing higher surface areas when NiO phase is present. Obviously, the higher the reduction temperature the lower the surface areas obtained for one particular caesium loading. We should have in mind that samples characterized by XRD were reduced under reactor conditions for 24 h, as given in the experimental section, and also the XRD technique as it only detects crystalline phases, a significant amorphous NiO content derived from its collapsing crystal reduction, may remain undetected.

The metallic particle sizes, calculated from the Scherrer equation, gave values of ca. 300–400 Å, as shown in Table 2. The method of Boudart [30] was also applied, for comparison, giving some 6-fold larger sizes than the former method. This discrepancy is generally obtained since the BET area method is highly sensible to surface aggregations of the crystallites, unlike the XRD technique which mainly detects the bulk structure and sizes of the composing single crystallites of an aggregation.

3.4. X-ray photoelectron spectroscopy

The X-ray photoelectron spectra of the catalysts prepared at one reduction temperature (523 K) with increasing caesium contents (samples 1,

Table 2
Ni particle/crystallite diameters (Å) of the reduced samples determined using different methods

Sample	BET [a]	XRD
4	972	330
5	2330	405
6	2654	417
8	1287	338
9	3698	409
10	3814	413
12	692	280
13	2439	407
14	2885	429

[a] Values obtained from the Boudard equation $S = 6/\rho d$, for cubic crystals.[b] Values obtained from the Scherrer equation $d = k\lambda / B \cos\theta$.

5, 9, 13 in Fig. 4) and those prepared with the intermediate caesium content at different reduction temperatures (samples 7, 8, 9, 10 in Fig. 5) were obtained.

From the experimental overall on-top curves, the decomposed peaks with the following binding energy values, 852.6, 854.1 and 862 eV were assigned to surface metallic nickel, Ni^{+2} species and its Ni^{+2} satellite, respectively. The non-stoichiometric Ni^{+3} species and its satellite may also appear at ca. 856 and 864.5 eV, respectively, mainly on partially reduced samples. Thus, an increase of the surface reduced nickel paralleling the increase of caesium content is depicted in Fig. 4, and the feature may be

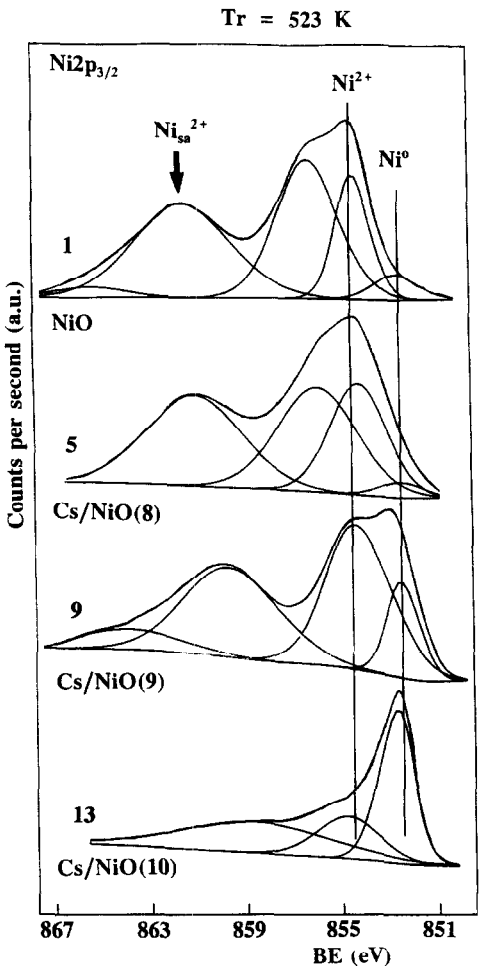

Fig. 4. X-ray photoelectron spectra of the $Ni_{2P_{3/2}}$ level for 1, 5, 9 and 13 nickel catalysts.

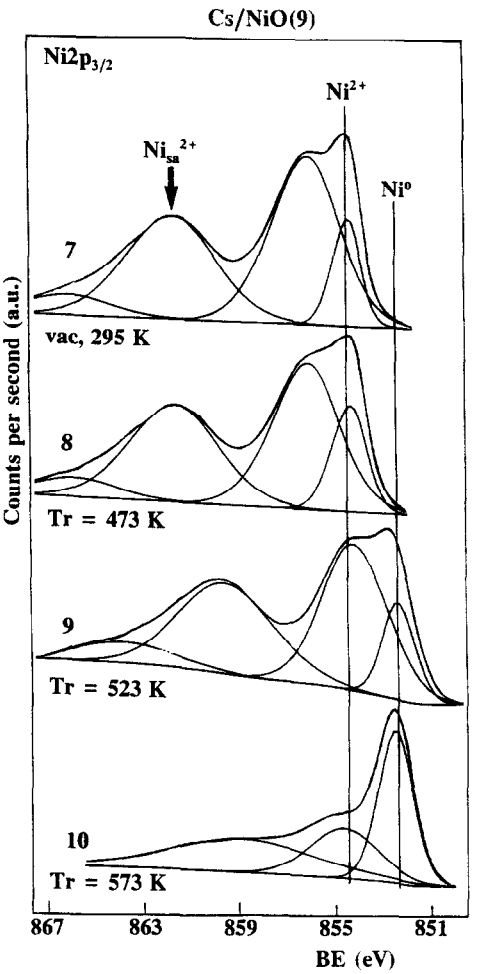

Fig. 5. X-ray photoelectron spectra of the $Ni_{2P_{3/2}}$ level for 7-10 nickel catalysts.

drawn that increasing caesium contents (in the range of intermediate and high caesium concentrations tested, catalysts 9, 13) promote the hydrogen NiO reduction at temperatures of 523 K and higher.

Fig. 5 shows the expected result that surface metal reduction increases with the increase of the reduction temperatures, being almost complete at 573 K for the intermediate caesium content on sample 10, and that no reduced surface nickel is detected at 473 K (sample 8, like sample 12 by XRD).

Table 3 depicts the quotient Cs/Ni atoms $\times 10^{-3}$ (chemical), as the initial chemical composition of the solids, the XPS intensities quo-

Table 3
Chemical analysis and XPS Cs/Ni surface atomic composition of the samples

Sample	Cs/Ni (chem. anal.) ($\times 10^{-3}$)	Surface I_{Cs}/I_{Ni} (XPS) ($\times 10^{-3}$)	Surface/ chemical
3	0.416	–	–
4	0.416	–	–
5	0.416	1.0	2.4
6	0.416	69.0	166.3
7	0.875	1.3	1.4
8	0.875	1.6	1.8
9	0.875	98.0	112.8
10	0.875	149.0	170.9
11	1.330	12.0	9.0
12	1.330	1003.0	754.0
13	1.330	1208.0	908.0
14	1.330	1386.0	1042.0

tient I_{Cs}/I_{Ni} atoms $\times 10^{-3}$ (surface) as a few layers thick surface composition, and the quotient of both expressed as surface/chemical composition.

Then, Table 3 shows a dramatic increase of caesium migration to the surface of the NiO solid on increasing the reduction temperature especially at those corresponding to the beginning of the reductions. Such loadings of surface caesium should bring about impediments or delays for the inwards hydrogen and outwards water diffusions during the NiO reduction process.

Under the reduction conditions below 473 K given in the experimental section, either non-reduction or an incipiently reduced material (less than 5% degree of reduction) is obtained. At this point very low concentration of Cs has been detected on the NiO surface by XPS. In turn, on reduction at temperatures higher than 473 K increasing Cs/Ni surface atomic ratios with increasing reduction temperatures are detected by XPS. Surface intensity ratios ranging between 1–1386 have been obtained (Table 3).

The cross sections and photoelectron mean free paths for NiO and zerovalent Ni, cannot explain only by themselves the intensity atomic ratios Cs/Ni of more than 1000 obtained, since the former show unrelevant differences for reduced Ni, Ni^{+2} and Ni^{+3} surface species (counts per second are given in arbitrary units).

Fig. 6. Scanning electron micrograph of the undoped NiO sample.

We then assume that high caesium concentration onto the NiO surface caused by aggregation effects from reduction (NiO surface area ~ 9 m^2/g versus reduced Ni surface area ~ 1.2 m^2/g) cooperatively with caesium migration to the surface caused by the water released during reduction should majorly account for the Cs/Ni surface ratios obtained since caesium oxide is a very hygroscopic material. Similar effects were found for other hygroscopic s-block doping elements.

3.5. Scanning electron microscopy

Scanning electron micrographs of the samples 1 and 12 are shown in Figs. 6 and 7,

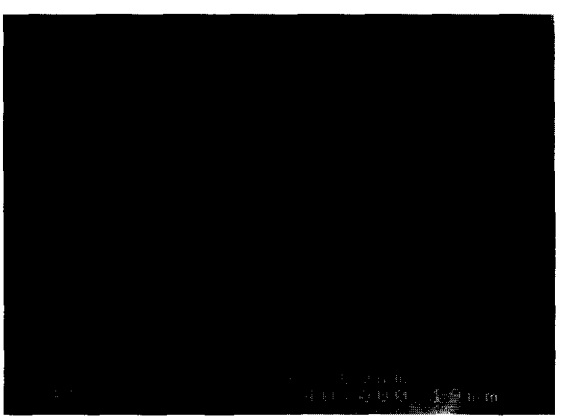

Fig. 7. Scanning electron micrograph of the caesium-doped NiO sample (3×10^{-3} g Cs_2O/g Ni). Reduced at 473 K.

respectively. Fig. 6 shows the characteristic quite uniformly crystallized NiO octahedra. However, the picture from Fig. 7 corresponding to the incipiently reduced caesium-doped sample 12 shows more round surfaces than those from undoped nickel, undoubtedly due to the collapse of the octahedra edges and vertex as being the preferred sites for the initial nickel nucleation, and also a small contribution to the surface octahedra deformation should presumably be detectable from the strong bulk caesium migration towards the surface of the solid under reduction, especially for the higher loaded caesium samples.

4. Conclusions

Several samples with potential interest as catalysts in hydrogenation reactions were obtained from doping NiO with different loading amounts of caesium oxide. The obtained solids were structurally characterized using BET, TPR, XRD, XPS and SEM techniques. From BET results, increasing caesium contents decrease surface areas except for those temperatures and caesium loadings giving rise to partial reductions. TPR shows that high caesium loadings can promote the beginning of NiO reduction, contrarily to previously reported potassium behaviors. TPR curves also display a reduction inhibiting counter-effect at the end of the reduction curves with the same increasing caesium loadings in line with the caesium migration towards the surface exhibited by XPS. XRD and SEM show differentiated crystalline morphologies on the oxidized and reduced caesium-doped nickel phases obtained from the solids studied. XPS plots display the reducibility behaviour of the solid surfaces confirming the NiO reduction promoting effect with increasing caesium loadings and also a dramatic caesium migration towards the surface of the solids mainly at the starting temperatures of reduction. That abundant surface caesium should delay the complete reduction of the solids and accounts for the TPR results and its seemingly contradictory behavior when compared with that from previously reported potassium.

References

[1] R.B. Anderson, in: Catalysis, P.H. Emmett (Ed.), Vol. IV, (Reinhold, New York, 1956) pp. 123; 332.
[2] W.D. Mross, Catal. Rev. Sci. Eng. 25 (1983) 591.
[3] M.E. Dry and G.J. Oosthuizen, J. Catal. 11 (1968) 18.
[4] R.B. Anderson, R.S. Karn and R.S. Shultz, J. Catal. 4 (1965) 56.
[5] H. Praliaud, J.A. Dalmon, C. Mirodatos and G.A. Martin, J. Catal. 97 (1986) 344.
[6] H. Praliaud, M. Primet and G.A. Martin, Appl. Surf. Sci. 17 (1983) 107.
[7] V. Pitchon, P. Gallezot, C. Nicot and H. Praliaud, Appl. Catal. 47 (1989) 357.
[8] M. Gravelle-Rumeau-Maillot, V. Pitchon, G.A. Martin and H. Praliaud, Appl. Catal. A 98 (1993) 45.
[9] G. Neri, A.M. Visco, A. Donato, C. Milone, M. Malentacchi and G. Gubitosa, Appl. Catal. A 110 (1994) 49.
[10] F. Medina, P. Salagre, J.L.G. Fierro and J.E. Sueiras, Appl. Catal. A 92 (1992) 131.
[11] F. Medina, P. Salagre, J.L.G. Fierro and J. and Sueiras, Solid State Ionics 59 (1993) 205.
[12] F. Medina, P. Salagre, J.L.G. Fierro and J.E. Sueiras, Appl. Catal. A 99 (1993) 115.
[13] F. Medina, P. Salagre, J.L.G. Fierro and J.E. Sueiras, J. Chem. Soc. Faraday Trans. 90 (1994) 1455.
[14] G.B. McVicker and M.A. Vannice, J. Catal. 63 (1980) 25.
[15] G.A. Somorjai, Catal. Rev. Sci. Eng. 23 (1981) 189.
[16] E.A. Blekkan, A. Holmen and S. Vada, Acta Chem. Scand. 47 (1993) 275.
[17] A. Cimino, M. Boudart and H. Taylor, J. Phys. Chem. 58 (1954) 796.
[18] A. Nielsen, Catal. Rev. Sci. Eng. 23 (1981) 17.
[19] M. Boudart, Catal. Rev. Sci. Eng. 23 (1983) 1.
[20] J.R. Rostrup-Nielsen, J. Catal. 33 (1974) 184.
[21] J.L. Johnson, Catal. Rev. Sci. Eng. 14 (1976) 131.
[22] E.B. Pereira and G.A. Martin, Appl. Catal. A 115 (1994) 135.
[23] D. Fried and D. Dollimore, J. Therm. Anal. 41 (1994) 323.
[24] J. Rasko, J. Bontovics and F. Solymosi, J. Catal. 146 (1994) 22.
[25] F. Medina, P. Salagre, J.L.G. Fierro and J.E. Sueiras, J. Mol. Catal. 81 (1993) 387.
[26] F. Medina, P. Salagre, J.L.G. Fierro and J.E. Sueiras, J. Catal. 142 (1993) 392.
[27] D. Simon and B. Bigot, Surf. Sci. 306 (1994) 459.
[28] J. Massardier, J.C. Bertolini, P. Ruiz and P. Delichère, J. Catal. 112 (1988) 21.
[29] J.L.G. Fierro, F. Medina, P. Salagre and J.E. Sueiras, J. Mol. Catal. 61 (1990) 187.
[30] M. Boudart and G. Djega-Mariadassou, Cinétique des Réaction en Catalyse Hétérogène, Masson, 1982, p. 26.